Assessment of thermal and electrical performance of flat plate air-cooled photovoltaic roof tile – experimental and numerical studies

Jakub Lukasik[1*], Jan Wajs[2]
[1,2]Gdańsk University of Technology, Faculty of Mechanical Engineering and Ship Technology, Institute of Energy
Narutowicza 11/12, 80-233 Gdańsk, Poland
[1]e-mail: jakub.lukasik@pg.edu.pl
[2]e-mail: jan.wajs@pg,edu.pl

Keywords: Photovoltaic roof tile, Building-Integrated Photovoltaic/Thermal (BIPV/T), Experimental study, Numerical simulations, Energy analysis

Abstract

The current state of development of the solar energy sector necessitates a new form of incentive for entities to invest in photovoltaic (PV) installations. Building-integrated photovoltaic/thermal (BIPV/T) systems are gaining increasing interest. Effective methods for heat recovery from BIPV/T collectors are searched for. Presented research experimentally and numerically considered the influence of cooling conditions on the electrical efficiency and heat recovery potential of PV roof tiles, using air as cooling medium. An experimental system consisted of PV roof tile module, casing and twenty halogen lamps, acting as a sunlight simulator. Temperature of PV roof tile and the casing, together with electrical current and voltage as well as volumetric air flow rate were controlled. Based on the experimental system, a numerical model was prepared in the ANSYS Fluent software. It takes into account two configurations of flow channel height 25 and 50 mm, various values of solar irradiance (from 300 to 900 W/m^2), and a set of different volumetric air flow rates (from 4.5 to 7.5 m^3/h). An approach based on the SST k-ω turbulence model and discrete ordinates (DO) radiation model was proposed. Among all the configurations investigated, the variant with a flow channel height of 25 mm exhibited a higher heat recovery potential. At extreme parameter values (solar irradiance of 900 W/m^2, volumetric air flow rate of 7.5 m^3/h), the highest heat flux, removed by the air, reached 330 W/m^2. The highest thermal efficiency, up to 48.7% and 44.2% for the (25 and 50 mm) channel height variants, respectively, was achieved at a solar irradiance of 300 W/m^2 and a volumetric air flow rate of 7.5 m^3/h. A high correspondence between experimental and numerical results was obtained, indicated by the root mean square percent error (RMSPE) of thermal efficiency at the range from 4.42% to 9.33%. The highest electrical efficiency (5.76%) was achieved for solar irradiance of 600 W/m^2 and a volumetric air flow rate of 7.5 m^3/h, for the variant with a channel height of 50 mm. These findings contribute to a better understanding of the influence of flow channel geometry and cooling conditions on module performance, supporting the design of more efficient and economically viable BIPV/T systems.

1 Introduction

In recent years, the photovoltaic (PV) sector has been one of the fastest growing branches of renewable energy sources (RES). The average worldwide growth rate of installed capacity in the years 2013-2022 was 22.33% year over year. A significant part of the PV market consists of prosumer installations placed on roofs or facades of buildings, operating as part of distributed generation. This method of mounting the modules gave rise to the idea of integrating photovoltaic installations with the building structure already at the design and construction stage [1], [2]. Building-integrated photovoltaics (BIPV) can replace classic roofing or building facades, but also act as windows, skylights or curtains in the case of semi-transparent building-integrated photovoltaic (STBIPV) modules [3], [4]. At the same time, a significant increase in the share of photovoltaics in the electricity production structure encourages to search for ways to improve the overall energy efficiency of the installation. Hybrid building-integrated photovoltaic/thermal (BIPV/T) systems enable heat recovery from the installation [5]. BIPV/T systems independently take over the functions dedicated to classic solar collectors and PV modules. They are characterized by a higher yield of useful energy in relation to the unit of occupied area.

Various methods of heat collection from BIPV/T installations are considered in the literature [6], [7]. The most common categories of cooling systems are the ones based on air, liquid, phase change of the working medium, as well as nanofluids and thermoelectric phenomena. The use of air is considered as the most practical solution in real applications. The numerous technical and economical advantages of air cooling have increased interest in this type of systems for commercial applications. However, the disadvantage of air cooling is a low heat transfer coefficient from the heat exchange surface. In order to increase the overall efficiency of the system, it is necessary to geometrically optimize the cooling system and search for cheap and effective techniques for heat removal intensification.

One of a classical air cooling systems applies forced convection and the air flow through a straight channel located under the backsheet of the module. Tests on the thermal and electrical efficiency of such a solution used for photovoltaic/thermal (PV/T) collectors were carried out by Dunne et al. [8]. Based on computational fluid dynamics (CFD) simulations, they found that increasing the channel height has a negative impact on the thermal and electrical efficiency achieved. A significant improvement in thermal and electrical efficiency is visible when the air flow velocity increases from 0.5 to 2.5 m/s. Above 2.5 m/s, no remarkable increase in energy benefits was observed. Hussien et al. [9] compared an experimental and numerical results of two air-cooled PV modules. In configuration no. 1, air flowed through a longitudinal channel located under the backsheet. In configuration no. 2, cooling was provided by a set of 8 small fans, blowing air perpendicular to the absorbing layer. Cooling with a longitudinal channel reduced the temperature on the module surface by 5.4 K and increased electrical efficiency by 1.34% compared to the uncooled module.

Comparative experimental studies of various designs of air PV/T collectors were conducted also by Chen et al. [10]. Closed structure with a glass cover (air flow under and over the PV module) and semi-closed structure without additional cover (air flow under the PV module) were compared. It was shown that the thermal and electrical efficiency of closed collectors increased by 11.6% and 19.4%, respectively, with an increase in the inlet air velocity of 1 m/s. Wu et al. [11] numerically investigated the effect of the flow channel position on the heat transfer characteristics and thermal-electric performance of an air-cooled PV/T system. A case with a glass channel located above the PV module (case 1) and a case with a channel located under the backsheet were considered (case 2). The average temperature of the PV module for case 2 was 18.44 K lower than for case 1. It was found that from the point of view of thermal and general efficiency and heat recovery potential, case 1 is a more advantageous solution. At the same time, from the point of view of electricity yield and electrical efficiency, case 2 turned out to be better than case 1.

The literature review shows that most studies concern classic PV modules or PV/T collectors. The research carried out in this work is devoted to the assessment of electrical and thermal benefits that can be obtained by using air-cooled PV roof tiles, which are consistent with the assumptions of BIPV/T systems. It is a continuation of work initiated several years ago [12]. The CFD simulations and experimental tests were performed for a wide range of input variables (volumetric air flow rate from 4.5 to 7.5 m^3/h; solar irradiance from 300 to 900 W/m^2). The analysis was carried out for two variants

of the flow channel height (H = 25 mm and H = 50 mm). The selected heights result from the limited availability of space in the case of integrating collectors with the roof covering and from the installation method of the tested roof tiles proposed by the manufacturer. Unlike in many literature items, attention was focused on examining low flow rates due to the considered possibility of integrating this type of systems with the evaporator of an air-source heat pump (ASHP).

2 Methodology

2.1 Experimental setup

Experimental research was carried out at a laboratory bench located at the Institute of Energy of the Gdańsk University of Technology. The subject of the research was the SolteQ Quad35 photovoltaic roof tile with PV cells made of monocrystalline silicon (m-Si). The basic technical data of the PV roof tiles used are presented in Table 1.

Table 1: Technical specification of the SolteQ Quad35 PV roof tile

Parameter	**Value**
Module dimensions	540 x 540 mm
Total area of the module	0.2916 m^2
Dimensions of the single cell	156 x 156 mm
Active area of the module	0.2190 m^2
Operating temperature	–40 to +80°C
Nominal power under STC	35 W ±3%
Operating voltage under STC	4.5 V
Operating current under STC	7.8 A
Unloaded voltage	4.9 V
Short-circuit current	8.2 A
Temperature coefficient of PV module	–0.5 ± 0.05%/K

The PV roof tile was placed in a sealed wooden casing. The lower part of the casing was a flow channel to which air was supplied through copper pipes. In order to increase the received heat flow, three wooden partitions were placed inside the channel to direct the flow of the medium. Depending on the tested height of the flow channel, a dedicated extension and partitions of appropriate height were used. Fig. 1 shows a diagram of the tested system with marked cell numbers.

The tile was illuminated using a solar light simulator consisting of 20 halogen lamps with 500 W of each filament. The selected halogen light is often used in laboratory tests as a substitute for solar radiation and reflects the real conditions at an acceptable level for research purposes [13], [14], [15]. The solar irradiance was measured by Kipp&Zonen CM6B pyranometer placed in the upper part of the roof tile casing. Due to the shift of the pyranometer relative to the center of the roof tile, the actual distribution of solar irradiance was measured at 9 reference points corresponding to the center of each cell. The obtained results were averaged and used as input parameters for the numerical model. The PV roof tile was placed on a frame and oriented perpendicular to the ground. This position of the roof tile allowed it to be directly illuminated by a solar light simulator, the front surface of which was parallel to the front surface of the PV module.

The air flow was forced by an external fan and measured with a rotameter. The surface temperature of the module was measured by the Fluke 62 Mini infrared thermometer at 9 measurement points, at which the solar irradiance value was controlled. Indications of this measuring instrument with a factory-set emissivity factor of 0.95 were corrected using a calibrated T-type thermocouple. This was to take into account the emissivity factor of the material from which the surface was made and adjust indications to the real conditions. The voltage was measured using Vorel 81780 multimeter, and the electrical current was measured by Emos EM391 multimeter.

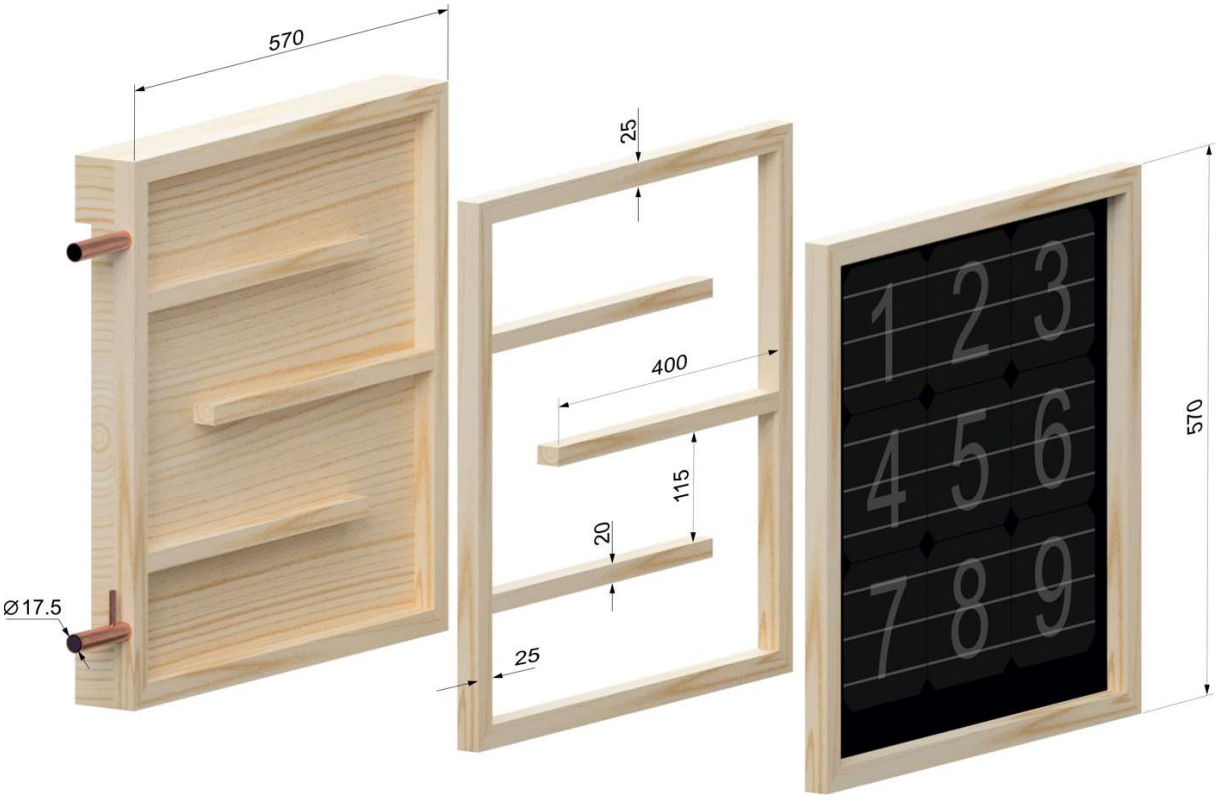

Figure 1: The casing of the tested PV roof tile

2.2 Mathematical formulation

The average temperature of the module was determined from the formula:

$$T_{surf\_avg} = \frac{\sum_{i=1}^{i=9} T_{surf\_i}}{n} \tag{1}$$

T_{surf_i} – front face temperature of the module at point i [K].

The power generated at the maximum power point (MPP) was calculated as:

$$P_{MPP} = U_{MPP} \cdot I_{e\_MPP} \tag{2}$$

U_{MPP} – voltage at MPP [V],
I_{e_MPP} – electrical current at MPP [A].

The electrical efficiency of the module was defined as:

$$\eta_{MPP} = \frac{P_{MPP}}{G \cdot A} \tag{3}$$

G – solar irradiance [W/m^2],
A – active area of the module [m^2].

The recovered heat flux was determined from the following formula:

$$q = \frac{\rho_{air\_avg} \cdot \dot{V} \cdot c_{avg} \cdot (T_{out} - T_{in})}{A_c} \tag{4}$$

ρ_{air_avg} – air density at average temperature between T_{in} and T_{out} [kg/m^3],

$\dot{V}$ – volumetric flow rate of air [m^3/s],
c_{avg} – average specific heat over a range of temperature values from T_{in} to T_{out} [J/(kg·K)],
T_{out} – temperature of the outlet air [K],
T_{in} – temperature of the inlet air [K],
A_c – total area of the module wetted by the cooling medium [m^2].

The CoolProp library of thermodynamic media [16] was used to determine the average density and average specific heat of the air. The thermal efficiency was related to the value of solar irradiance incident on the module and was calculated as follows:

$$\eta_{th} = \frac{q}{G} \tag{5}$$

2.3 Numerical model

The numerical analysis was performed in the ANSYS Fluent 2021 R1 software. The prepared geometry reflected the experimental setup. A locally refined conformal tetragonal mesh was prepared. Meshes up to 3,020,000 cells for channel height of 25 mm and 3,233,200 cells for channel height of 50 mm were tested. After conducting the mesh sensitivity study, the final adapted mesh consisted of 949,000 cells for the variant with a 25 mm high channel and 1,168,000 cells for the variant with a 50 mm channel height. Averaged skewness was at the level of 0.25 for 25 mm and 0.24 for 50 mm channel height. In the fluid-solid contact zone, within boundary layer, 10 rows of elements were generated, introduced using a fixed growth rate of 1.2. The average values of the y+ parameter were equal to 1.17 for the case with 25 mm and 1.60 for the case with 50 mm channel height. Constant values of the thermophysical material properties were assumed. The air density was the exception and was calculated using the Boussinesq approximation, with a given thermal expansion coefficient of 0.0034 K^{-1}.The thermal-flow model was solved using the finite volume method (FVM), based on the equations of continuity, momentum and energy [17], [18]. Due to the range of Reynolds numbers covering laminar and turbulent flow, the SST *k-ω* turbulence model was used. The Reynolds number was defined as:

$$Re = \frac{\rho \cdot v \cdot D_h}{\mu} \tag{6}$$

v – velocity magnitude [m/s],
D_h – hydraulic diameter of the air duct [m],
μ – dynamic viscosity [kg/(m·s)].

The hydraulic diameter was defined as:

$$D_h = \frac{4A_f}{P} \tag{7}$$

A_f – cross-sectional area of the flow [m^2],
P – wetted perimeter of the cross-section [m].

The turbulence intensity at the inlet was determined by the formula [8]:

$$I_t = 0.16 \cdot Re^{-\frac{1}{8}} \tag{8}$$

To model solar radiation falling on the front surface of a PV roof tile, the discrete ordinates radiation model was used, enabling the modeling of semi-transparent layers. It is based on the solution of the radiative transfer equation (RTE), which determines the intensity of radiation I transported from position $\vec{r}$ towards direction $\vec{s}$, which is defined as [17], [18]:

$$\frac{dI(\vec{r},\vec{s})}{ds} = -(a+\sigma_s)I(\vec{r},\vec{s}) + a\frac{{n_{ref}}^2\sigma T^4}{\pi} + \frac{\sigma_s}{4\pi}\int_0^{4\pi} I(\vec{r},\vec{s}')\Phi(\vec{s}\cdot\vec{s}')d\Omega' \quad (9)$$

I – radiation intensity [W/m^2],
$\vec{r}$ – position vector [m],
$\vec{s}$ – unit vector in direction of scattering [-],
s – path length [m],
a – absorption coefficient [1/m],
σ_s – scattering coefficient [1/m],
n_{ref} – refractive index [-],
σ – Stefan-Boltzmann constant [W/(m^2·K^4)],
$\vec{s}'$ – unit vector in the direction of the incident radiation [-],
Φ – phase function [-],
Ω – solid angle [sr].

The heat transfer coefficient from the front surface of the module was defined according to the formula [19], [20]:

$$h_{nat} = 1.78 \cdot \left(T_{surf\_avg} - T_{amb\_PV}\right)^{\frac{1}{3}} \quad (10)$$

T_{amb_PV} – temperature in a vicinity of the PV roof tile [K].

The following assumptions were made:

- external radiation incident on the module and casing was perpendicular to the front surface and was considered as a direct radiation (no reflected radiation);
- layers of the modules (glass, ethylene-vinyl acetate (EVA) film, silicon, polyvinyl-fluoride (PVF)) were modelled, taking into account properties of each material and thicknesses of layers,
- only glass and EVA film were treated as a semi-transparent solid materials;
- the radiative heat transfer mechanism was assumed on all external and internal walls;
- the conversion of solar radiation into electricity in silicon cells was not taken into account in the thermal flow calculations;
- boundary conditions at the inlet were taken from experiment in the form of a constant temperature equal to the measured inlet temperature and a uniform velocity;
- the boundary condition at the outlet was given in the form of a constant value of atmospheric pressure (101,325 Pa);
- all walls were treated as no-slip;
- the thermophysical properties of the materials did not depend on temperature (except for air density).

3 Results and discussion

3.1 Experimental results

The tests were carried out in the range of volumetric flow rates from 4.5 to 7.5 m^3/h, in steps of 1.5 m^3/h. These flow rates correspond to Reynolds numbers defined at the cross-sectional area between lower wall of the casing and the first partition ranging from 2564 to 4273, for cases with a 25 mm channel height, and from 1511 to 2518, for cases with 50 mm channel height. The reference configuration was a system without cooling. Figure 2 presents the profiles of the average temperature on the front surface of the module and the profiles of the electrical efficiency of the PV roof tile obtained for both tested heights of the flow channel, presented as a function of solar irradiance.

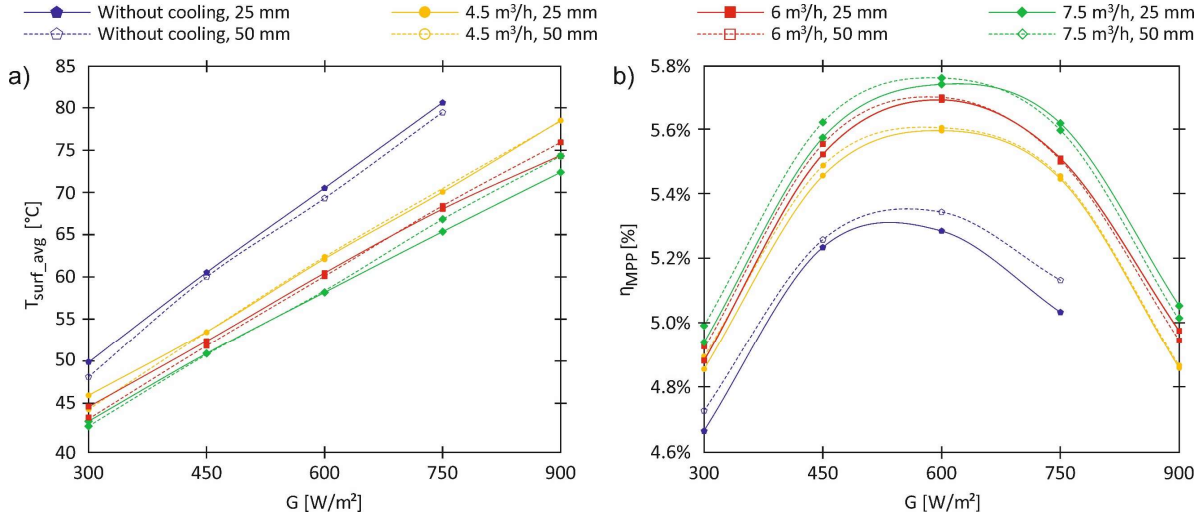

Figure 2: Experimental results of: (a) temperature profiles of the PV module front surface; (b) electrical efficiency as a function of solar irradiance

In the whole range of volumetric flow rates, at low values of solar irradiance (300-450 W/m^2), lower operating temperature is obtained in the case of a duct with a height of 50 mm. As solar irradiance increases, the average temperature values of the module for both duct heights begin to equalise (at approx. 600 W/m^2). Above 600 W/m^2, the configuration with a lower duct height causes a lower operating temperature. It comes from higher values of velocity of the air flowing through a duct with a lower height. A shorter time of air contact with the hot absorbing layer reduces the temperature of the fluid, and thus improves the conditions for heat removal, lowering the module temperature to a greater extent. At low values of solar irradiance, the backsheet temperature is not so high, and the impact of this phenomenon is limited. The family of experimentally obtained characteristics of recovered heat flux and thermal efficiency of PV roof tile are presented in Fig. 3.

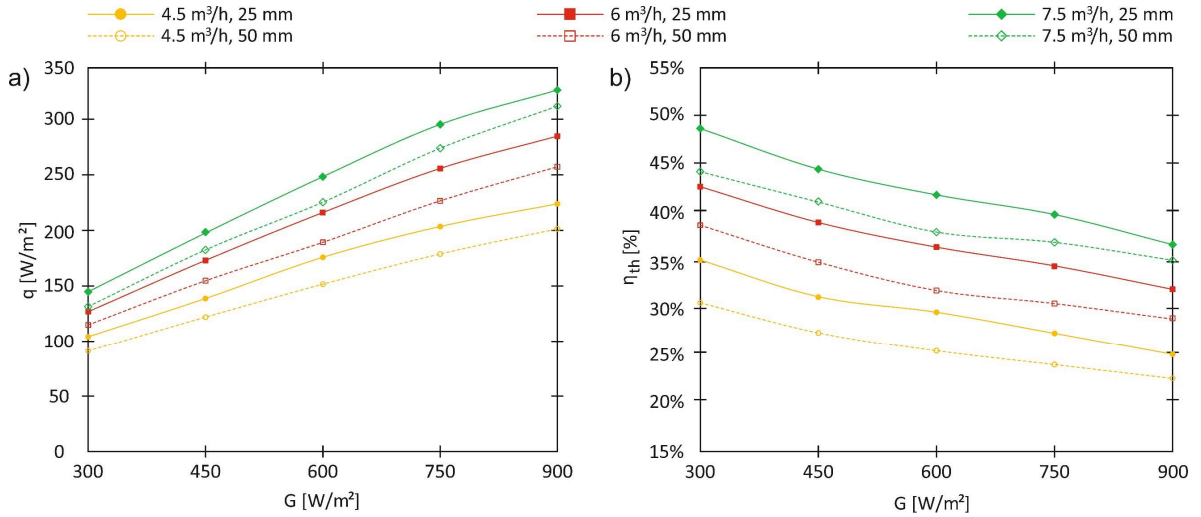

Figure 3: Experimental characteristics of: (a) heat flux received by cooling air; (b) thermal efficiency of PV roof tile as a function of solar irradiance

The results show that in each of the cases analyzed, the flow duct with a height of 25 mm allows for more effective heat recovery. The maximum value of the heat flux was 329.8 W/m^2. It was received for a solar irradiance of 900 W/m^2 and volumetric air flow rate of 7.5 m^3/h. The coefficients of the linear regression determination R^2 for each characteristic range from 0.9879 to 0.9983. In the case of thermal efficiency, its decrease is visible with increasing solar irradiance. This is due to the decreasing share of energy that can be received by the cooling air.

3.2 CFD results

As in the case of experimental studies, the characteristics obtained numerically were plotted as a function of the solar irradiance. Figure 4 shows the received heat flux and thermal efficiency of the PV roof tile. At this stage, the CFD simulations focused only on the thermal aspect, so the electrical and overall efficiency characteristics were not taken into account.

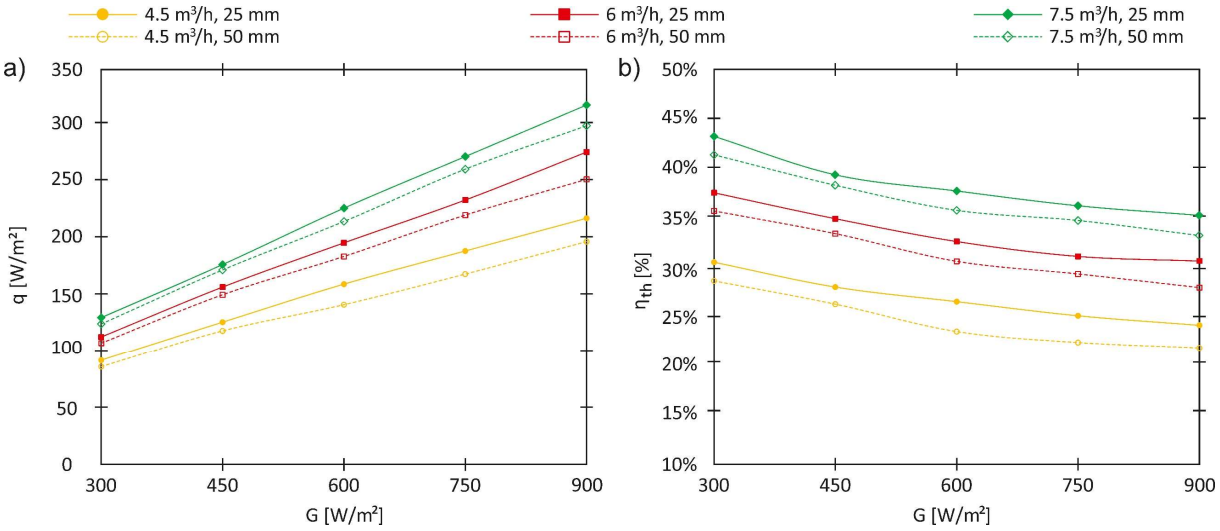

Figure 4: Numerical characteristics of: (a) heat flux received by the cooling air; (b) thermal efficiency of the PV roof tile as a function of solar irradiance

The characteristics are similar to those obtained from the experiment. To assess the quality of the numerical model and the degree of the mapping of experimental data, an averaged relative difference in the values of selected parameters (δ_i), as well as root mean square percent error (RMSPE) were determined for each case analyzed. They were calculated according to the following formulas [8], [21]:

$$\delta_i = \frac{x_{CFD,i} - x_{ex,i}}{x_{ex,i}} \tag{11}$$

$$RMSPE = \sqrt{\frac{1}{N} \cdot \sum_{i=1}^{N} (100 \cdot \delta_i)^2} \tag{12}$$

$x_{CFD,i}$ – value of the parameter obtained from CFD calculations,
$x_{ex,i}$ – value of the parameter obtained from the experiment,
N – number of data sets [-].

Table 4 shows the relative differences and RMSPE between the thermal results obtained for each series with different volumetric air flow rate values, averaged for analyzed range of solar irradiance.

Table 4: Relative differences and RMSPE between numerical and experimental results

$\dot{V}$	H	δ of the t_{surf_avg}	$RMSPE$ of the t_{surf_avg}	δ of the q and η_{th}	$RMSPE$ of the q and η_{th}
4,5 m³/h	25 mm	0,33%	0.40%	-8.74%	9.24%
	50 mm	0,39%	0.51%	-5,30%	5.56%
6 m³/h	25 mm	0,34%	0.47%	-8.94%	9.33%
	50 mm	0,43%	0.52%	-4,12%	4.42%
7,5 m³/h	25 mm	0,39%	0.45%	-8,70%	9.15%
	50 mm	0,36%	0.44%	-5,60%	5.63%

Slight overestimation of the average front surface temperature in the numerical results was found in each considered volumetric air flow rate. Differences at the level of a few percent are also visible in the case of the heat flux and thermal efficiency. The differences are mainly attributed to factors such as: the use of halogen light simulator with a slightly different emission spectrum than sunlight; the nonuniformity of the distribution of solar irradiance on the surface of the PV roof tile; the use of an averaged value of the convective heat transfer coefficient for the face of the PV module, the impossibility of obtaining an ideal steady state, measurement uncertainties of the considered quantities, potential differences in the thermophysical properties of the materials used, deviations in the position of the temperature measurement point at the outlet of the air flow channel relative to the pipe axis. However, the similarity of the results obtained for both research paths can be considered high (RMSPE < 0.6% for the averaged absolute temperature of PV module surface and RMSPE < 10% for the heat flux and thermal efficiency).

Figure 5 shows the front surface temperature distribution. The points where the temperature was controlled were marked with a black plus sign. The numerical results are presented for conditions of the solar irradiance of 600 W/m^2 and volumetric air flow rate equal to 7.5 m^3/h.

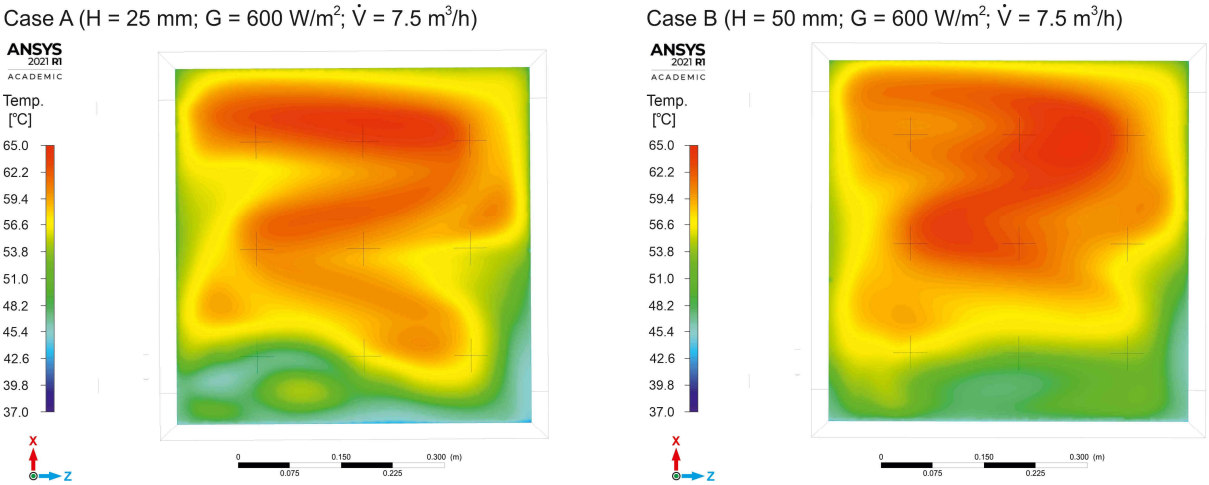

Figure 5: Temperature distribution on the front surface of the PV roof tile: case A for channel height equal to 25 mm; case B for channel height equal to 50 mm

Figure 6 presents the velocity distribution in the longitudinal cross-section (*xz*), located 2 mm below the backsheet of the module. Figure 7 shows the velocity distribution in the transverse cross-section (*xy*) located in the middle of the airflow channel, equidistant from the left and right casing walls.

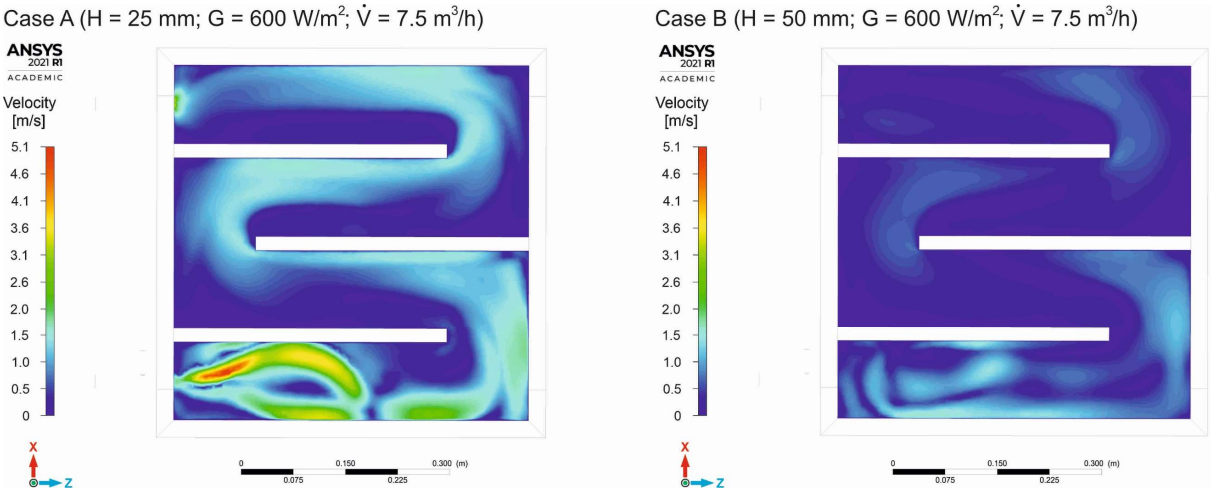

Figure 6: Velocity distribution in the longitudinal cross-section (xz) located 2 mm below the backsheet of the PV roof tile: case A for channel height equal to 25 mm; case B for channel height equal to 50 mm

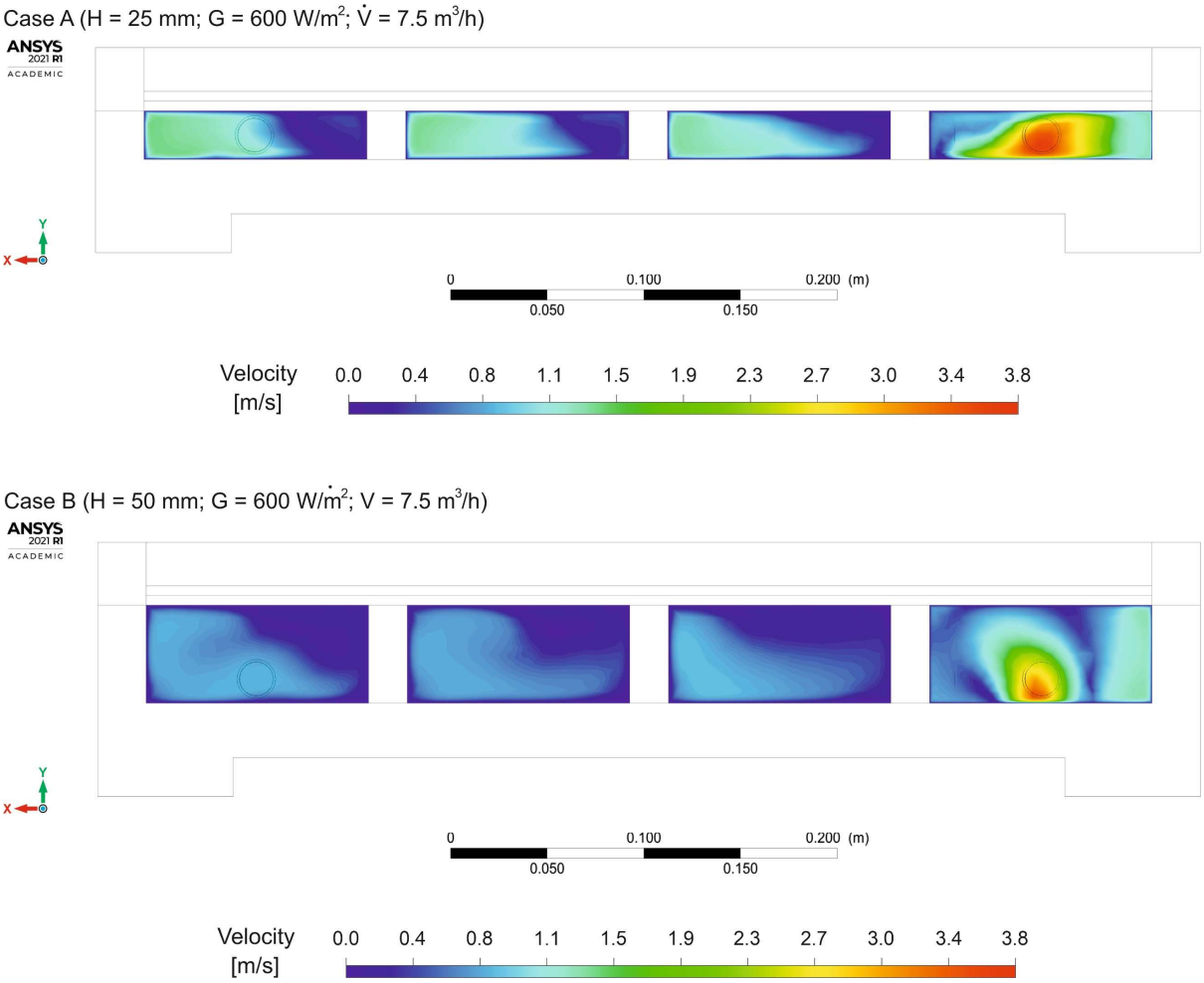

Figure 7: Velocity distribution in the transverse cross-section (xy) located in the middle of the airflow channel: case A for channel height equal to 25 mm; case B for channel height equal to 50 mm

The greatest difference in temperature distribution on the front surface of the PV module between channels with heights of 25 and 50 mm occurs in the area of cells nos. 7-9 (see Fig. 1), located in the lower part of the module. This area is characterized by a different distribution of velocity of cooling air. In the channel with a lower height, the main air stream flows from the inlet pipe towards the lower casing wall. Figure 5 clearly shows the zone of low temperature values in the main flow stream area. Near cell no. 8, the main flow stream deflects towards the bottom wall and then changes direction due to the partition.

For a channel height of 50 mm, the main flow stream follows the *z*-axis towards the right-hand side wall after leaving the inlet pipe. Under cells nos. 7-9, the air velocity near the module's backsheet is significantly lower than in the 25 mm channel. The main air stream interacting with the module's backsheet is much less visible. After passing the first partition, the streamlines are similar in both channels. However, in the *xz* cross-section, the velocity of the main stream is lower in the 50 mm channel. In both channels, after bypassing the first partition, air mixing in the *y*-axis direction results in a more uniform velocity distribution along the channel height compared to the area below the first partition. Stagnation areas are visible in both channels occurring near the left casing wall at the level of the second partition and near the right casing wall at the level of the third partition.

4 Conclusions

The paper presents the results of research on the influence of air cooling conditions of a photovoltaic roof tile and the height of the flow channel (25 and 50 mm) on its electrical and thermal efficiency.

The motivation to carry out work in this area was a pertinence of forced cooling of BIPV/T modules, which are particularly exposed to operation at elevated temperatures. A literature gap was found among works dedicated to this type of system, which would comprehensively address the issues of the influence of the height of the flow channel and other input variables on the obtained results. Continuing the work carried out by the authors, the focus was on the development of a dedicated numerical model and its verification using an experimental stand.

The results obtained by both approaches confirmed a significant impact of the considered input variables on the obtained performance indicators. It was found that the height of the flow channel has a great influence on the possibility of heat recovery, but a small one on the achieved electrical efficiency. The maximum relative increase in electrical efficiency thanks to the use of cooling was 11.73%. It was obtained for an air duct height of 25 mm, at a solar irradiance of 750 W/m^2 and an air flow rate of 7.5 m^3/h. The system with the highest thermal potential turned out to be the configuration with a channel height of 25 mm. The highest heat flux was 329.84 W/m^2 and was obtained at a solar irradiance of 900 W/m^2 and a volumetric flow rate of 7.5 m^3/h. Under the same cooling conditions, but with a solar irradiance of 300 W/m^2, the highest thermal efficiency value was 48.70%. It has been proven that a higher flow rates increases the removed heat flux and improves the thermal efficiency.

A high correspondence between the experimental results and the CFD simulation results was highlighted. The average relative differences between the parameters considered were at the level of several percent. RMSPE was lower than 10% in case of thermal efficiency and lower than 0.6% for average absolute temperature of PV module surface. Thus, the usefulness of the model for further research was demonstrated. Differences in a flow structure have consequences in a form of higher thermal efficiency values and increased heat recovery potential for a configuration with a lower channel height. The presented research contributes to filling the literature gap and helps to understand the phenomena occurring in photovoltaic/thermal systems.

References

[1] J. A. Clarke, J. W. Hand, C. M. Johnstone, N. Kelly, and P. A. Strachan, 'Photovoltaic-integrated building facades', *Renewable Energy*, vol. 8, no. 1, pp. 475–479, May 1996, doi: 10.1016/0960-1481(96)88902-6.

[2] T. Yang and A. K. Athienitis, 'A review of research and developments of building-integrated photovoltaic/thermal (BIPV/T) systems', *Renewable and Sustainable Energy Reviews*, vol. 66, pp. 886–912, Dec. 2016, doi: 10.1016/j.rser.2016.07.011.

[3] A. S. Abdelrazik, B. Shboul, M. Elwardany, R. N. Zohny, and A. Osama, 'The recent advancements in the building integrated photovoltaic/thermal (BIPV/T) systems: An updated review', *Renewable and Sustainable Energy Reviews*, vol. 170, p. 112988, Dec. 2022, doi: 10.1016/j.rser.2022.112988.

[4] E. Gaucher-Loksts, A. Athienitis, and M. Ouf, 'Design and energy flexibility analysis for building integrated photovoltaics-heat pump combinations in a house', *Renewable Energy*, vol. 195, pp. 872–884, Aug. 2022, doi: 10.1016/j.renene.2022.06.028.

[5] C. Şirin, J. Goggins, and M. Hajdukiewicz, 'A review on building-integrated photovoltaic/thermal systems for green buildings', *Applied Thermal Engineering*, vol. 229, p. 120607, Jul. 2023, doi: 10.1016/j.applthermaleng.2023.120607.

[6] K. Bilen and İ. Erdoğan, 'Effects of cooling on performance of photovoltaic/thermal (PV/T) solar panels: A comprehensive review', *Solar Energy*, vol. 262, p. 111829, Sep. 2023, doi: 10.1016/j.solener.2023.111829.

[7] M. Herrando *et al.*, 'A review of solar hybrid photovoltaic-thermal (PV-T) collectors and systems', *Progress in Energy and Combustion Science*, vol. 97, p. 101072, Jul. 2023, doi: 10.1016/j.pecs.2023.101072.

[8] N. A. Dunne, P. Liu, A. F. A. Elbarghthi, Y. Yang, V. Dvorak, and C. Wen, 'Performance evaluation of a solar photovoltaic-thermal (PV/T) air collector system', *Energy Conversion and Management: X*, vol. 20, p. 100466, Oct. 2023, doi: 10.1016/j.ecmx.2023.100466.

[9] A. Hussien, A. Eltayesh, and H. M. El-Batsh, ‘Experimental and numerical investigation for PV cooling by forced convection’, *Alexandria Engineering Journal*, vol. 64, pp. 427–440, Feb. 2023, doi: 10.1016/j.aej.2022.09.006.
[10] Y. Chen *et al.*, ‘A comparative experimental study on the performance of photovoltaic thermal air collectors’, *Applied Thermal Engineering*, p. 123109, Apr. 2024, doi: 10.1016/j.applthermaleng.2024.123109.
[11] S.-Y. Wu, T. Wang, L. Xiao, and Z.-G. Shen, ‘Effect of cooling channel position on heat transfer characteristics and thermoelectric performance of air-cooled PV/T system’, *Solar Energy*, vol. 180, pp. 489–500, Mar. 2019, doi: 10.1016/j.solener.2019.01.043.
[12] J. Wajs, A. Golabek, and R. Bochniak, ‘Photovoltaic Roof Tiles: The Influence of Heat Recovery on Overall Performance’, *Energies*, vol. 12, no. 21, Art. no. 21, Jan. 2019, doi: 10.3390/en12214097.
[13] ‘SIN PP | Widmowo–termiczne aspekty symulacji promieniowania słonecznego’. Accessed: Apr. 08, 2024. [Online]. Available: https://sin.put.poznan.pl/dissertations/details/d394
[14] ‘Standard Specification for Solar Simulation for Photovoltaic Testing’. Accessed: Feb. 06, 2024. [Online]. Available: https://www.astm.org/e0927-10r15.html
[15] H. Moria, T. I. Mohamad, and F. Aldawi, ‘Radiation distribution uniformization by optimized halogen lamps arrangement for a solar simulator’, *J Sci Eng Res*, vol. 3, pp. 29–34, 2016, Accessed: Apr. 08, 2024. [Online]. Available: http://scholars.utp.edu.my/id/eprint/36638/
[16] ‘Welcome to CoolProp — CoolProp 6.6.0 documentation’. Accessed: Apr. 10, 2024. [Online]. Available: http://www.coolprop.org/
[17] M. Pawlucki, M. Krys, 'CFDs for engineers. Practical exercises on the example of the Ansys Fluent system' (in Polish), Helion SA, Gliwice, 2020, pp. 249-256.
[18] T. Hân, ‘ANSYS Fluent Theory Guide’, Accessed: Apr. 09, 2024. [Online]. Available: https://www.academia.edu/33546431/ANSYS_Fluent_Theory_Guide
[19] S. Sandooghdar, S. Akbarzadeh, M. S. Valipour, and A. Arabkoohsar, ‘Performance improvement of air-based solar photovoltaic/thermal collectors using wavy channels’, *Renewable Energy*, vol. 211, pp. 831–845, Jul. 2023, doi: 10.1016/j.renene.2023.05.043.
[20] C. Kalkan, M. A. Ezan, J. Duquette, Ş. Yilmaz Balaman, and A. Yilanci, ‘Numerical study on photovoltaic/thermal systems with extended surfaces’, *International Journal of Energy Research*, vol. 43, no. 10, pp. 5213–5229, 2019, doi: 10.1002/er.4477.
[21] M. Shcherbakov, A. Brebels, A. Tyukov, T. Janovsky, and V. Anatol, ‘A Survey of Forecast Error Measures’, 2013. Accessed: Apr. 11, 2024. [Online]. Available: https://www.semanticscholar.org/paper/A-Survey-of-Forecast-Error-Measures-Shcherbakov-Brebels/435eb6e05fcda264c8c1e7fbcdee7116bb5b1424?p2df